Atmos. Chem. Phys., 14, 8933–8946, 2014
www.atmos-chem-phys.net/14/8933/2014/
doi:10.5194/acp-14-8933-2014

Atmospheric Chemistry and Physics
Open Access

Kinetics of the reactions of isoprene-derived hydroxynitrates: gas phase epoxide formation and solution phase hydrolysis

M. I. Jacobs, W. J. Burke, and M. J. Elrod

Department of Chemistry and Biochemistry, Oberlin College, Oberlin, Ohio, USA

Correspondence to: M. J. Elrod (mjelrod@oberlin.edu)

Received: 28 April 2014 – Published in Atmos. Chem. Phys. Discuss.: 13 May 2014
Revised: 16 July 2014 – Accepted: 22 July 2014 – Published: 1 September 2014

Abstract. Isoprene, the most abundant non-methane volatile organic compound (VOC) emitted into the atmosphere, is known to undergo gas phase oxidation to form eight different hydroxynitrate isomers in "high-NO_x" environments. These hydroxynitrates are known to affect the global and regional formation of ozone and secondary organic aerosol (SOA), as well as affect the distribution of nitrogen. In the present study, we have synthesized three of the eight possible hydroxynitrates: 4-hydroxy-3-nitroxy isoprene (4,3-HNI) and E / Z-1-hydroxy-4-nitroxy isoprene (1,4-HNI). Oxidation of the 4,3-HNI isomer by the OH radical was monitored using a flow tube chemical ionization mass spectrometer (FT-CIMS), and its OH rate constant was determined to be $(3.64 \pm 0.41) \times 10^{-11}$ cm^3 molecule^{-1} s^{-1}. The products of 4,3-HNI oxidation were monitored, and a mechanism to explain the products was developed. An isoprene epoxide (IEPOX) – a species important in SOA chemistry and thought to originate only from "low-NO_x" isoprene oxidation – was found as a minor, but significant, product. Additionally, hydrolysis kinetics of the three synthesized isomers were monitored with nuclear magnetic resonance (NMR). The bulk, neutral solution hydrolysis rate constants for 4,3-HNI and the 1,4-HNI isomers were $(1.59 \pm 0.03) \times 10^{-5}$ s^{-1} and $(6.76 \pm 0.09) \times 10^{-3}$ s^{-1}, respectively. The hydrolysis reactions of each isomer were found to be general acid-catalyzed. The reaction pathways, product yields and atmospheric implications for both the gas phase and aerosol phase reactions are discussed.

1 Introduction

Isoprene (2-methyl-1,3-butadiene) is a volatile alkene produced mainly by deciduous trees and shrubs whose global emissions have been estimated at 600 Tg yr^{-1} (Guenther et al., 2006), making it the most abundant non-methane volatile organic compound (VOC) in the atmosphere. Because of its abundance and two double bonds (which make it particularly susceptible to oxidation by species such as the OH radical or ozone), isoprene oxidation is important in the formation of both ozone and secondary organic aerosols (SOAs) (Carlton et al., 2009).

Hydroxynitrates are produced from isoprene oxidation in "high-NO_x" environments (Lockwood et al., 2010; Paulot et al., 2009a). Organic nitrates are products of the reaction between peroxyradicals (ROO) and nitric oxide (NO), and their formation is highly dependent on the alkyl chain length (Atkinson, 1990). The total (non-isomer-specific) yield of the isoprene-derived hydroxynitrates has been measured several times, and the measurements span a very large range (from 4.4 to 15 %) (Chen et al., 1998; Chuong and Stevens, 2002; Patchen et al., 2007; Paulot et al., 2009a; Sprengnether et al., 2002). Because the formation of the hydroxynitrates results in the sequestration of NO_x, the large variation in the estimated yields of hydroxynitrates has profound implications for the assessments of ozone production caused by isoprene photooxidation (Fiore et al., 2005; Horowitz et al., 2007; von Kuhlmann et al., 2004). The eight possible isomers of isoprene-derived hydroxynitrates and their estimated relative yields (Paulot et al., 2009a) are given in Table 1.

The ability of the hydroxynitrates to sequester NO_x depends on the details of their atmospheric fate. The production of organic nitrates creates compounds with a lower vapor pressure that are more hydrophilic than their precursor

Table 1. Isoprene-derived hydroxynitrate isomers with their calculated yields (Paulot et al., 2009a).

Structure	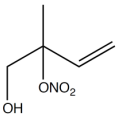	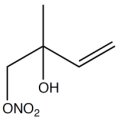	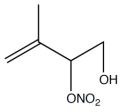	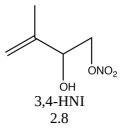
Abbreviation	1,2-HNI	2,1-HNI	4,3-HNI	3,4-HNI
Yield (%)	23.1	1.1	12.8	2.8
Structure	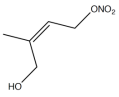	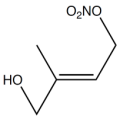	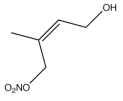	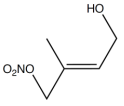
Abbreviation	(Z)-1,4-HNI	(E)-1,4-HNI	(Z)-4,1-HNI	(E)-4,1-HNI
Yield (%)	4.6	26.5	4.4	24.8

volatile organic compounds. Thus, organic nitrates are believed to play an important role in SOA chemistry. Ambient aerosol measurements have indicated that 17–23 % of molecules in organic aerosol contain the $RONO_2$ functional group (Rollins et al., 2013). Laboratory studies have indicated that tertiary organic nitrates undergo fast hydrolysis under typical aerosol conditions (Darer et al., 2011; Hu et al., 2011). Recent studies have shown that the partitioning of hydroxynitrates into the particle phase is strongly dependent on the relative humidity; at high RH, α-pinene-derived hydroxynitrates and their hydrolysis products have been observed in SOA (Rindelaub et al., 2014). Uptake into SOA represents a permanent sequestration of NO_x from the gas phase, which leads to a decrease in ozone production associated with hydroxynitrates.

However, further gas phase oxidation of hydroxynitrates is possible, and, depending on the rate of OH reaction and the product formation mechanism, they may recycle NO_x back into the gas phase. A previous chamber study that investigated the oxidation of isoprene in a high-NO_x environment predicted that 60–70 % of all hydroxynitrates release NO_x when further oxidized by the OH radical (Paulot et al., 2009a). If the gas phase oxidation is slow and occurs on a long enough timescale, hydroxynitrates may be transported significant distances from the source region to a remote location where the subsequent recycling of NO_x can result in accelerated photochemistry and enhanced ozone formation (Paulot et al., 2012). Understanding how the isoprene-derived hydroxynitrates might react in both the aerosol phase – leading to permanent NO_x sequestration – and gas phase – which could lead to the release of NO_x into the gas phase – is important for the refinement of air quality models.

In the present research, we have synthesized some of the isoprene-derived hydroxynitrates to study their possible atmospheric fates: gas phase oxidation and aerosol phase uptake. Three isoprene-derived hydroxynitrates – 4-hydroxy-3-nitroxy isoprene (4,3-HNI) and E / Z 1-hydroxy-4-nitroxy isoprene (E / Z 1,4-HNI) – have been synthesized. The OH radical rate constant for 4,3-HNI oxidation has been measured using our lab's flow tube chemical ionization mass spectrometer (FT-CIMS), and a mechanism to explain the observed products has been proposed. Additionally, the hydrolysis rate constants in neutral, bulk aqueous solution have been measured using nuclear magnetic resonance (NMR) as the analytical technique. The oxidation and hydrolysis kinetics of a similar, unsaturated hydroxynitrate (1-hydroxy-2-nitroxy-3-butene (1,2-HNB)) were also investigated in order to explore the generality of mechanisms gleaned from similar study of the isoprene-derived species.

2 Experimental

2.1 Synthesis of hydroxynitrates

The methods used in the syntheses of 4,3-HNI; E / Z 1,4-HNI; and 1-hydroxy-2-nitroxy-3-butene (1,2-HNB) are given in the Supplement.

2.2 NMR technique

Hydroxynitrate hydrolysis was studied using an NMR-based technique previously developed in our lab (Darer et al., 2011). Hydrolysis of the various hydroxynitrate species was monitored using ^{1}H NMR (eight scans, 30 s). Chemical shifts were calibrated relative to the solvent monodeuterated water (HDO) peak (4.79 ppm) for all ^{1}H spectra. The kinetics spectra were collected in aqueous solutions prepared from 99.9 % D_2O (Cambridge Isotope Lab, Inc.) and 68 wt % $DClO_4$ (Sigma-Aldrich).

2.3 Hydroxynitrate hydrolysis experiments

Hydrolysis kinetics measurements were made by collecting sequential ^{1}H NMR spectra over the course of the hydrolysis experiment (times varied for different isomers) and measuring the depletion of the hydroxynitrates. Each measurement was performed in the same manner: 10 µL of hydroxynitrate

were added to a 1 mL aliquot of the desired aqueous solution, and the solution was stirred in a 10 mL beaker. After approximately 1 min of stirring to ensure solution homogeneity, the entire reaction mixture was loaded into an NMR tube, and spectral collection was started. For 1,4-HNI, the relative 1,4-HNI concentration was determined by comparing the nitrate proton peak (5.00 ppm) relative to an internal standard (2,2-dimethyl-2-silapentane-5-sulfonate sodium salt, DSS, which had a nine-proton peak at 0.00 ppm). For 4,3-HNI, the relative 4,3-HNI concentration was determined by comparing the 4,3-HNI methyl group protons (1.81 ppm) to the product methyl group protons (1.64, 1.69 and 1.71 ppm). For 1,2-HNB, the relative 1,2-HNB concentration was determined by comparing the 1,2-HNB alcohol group protons (3.8 ppm) to the equivalent product alcohol group protons (3.54 ppm). A first-order decay rate law was found to fit the organic hydroxynitrate concentration vs. time data, and the first-order rate constants (and thus the lifetimes) of the species were determined.

2.4 HNI gas phase oxidation experiments

2.4.1 Flow tube apparatus

A schematic of the flow tube apparatus is given in Fig. 1 and is similar to the instrument configuration used in a previous study of the OH reaction with isoprene-derived epoxides (Jacobs et al., 2013). The main flow tube was 100 cm in length and constructed with 2.2 cm inner diameter Pyrex tubing. A large flow of O_2 carrier gas (15 STP L min^{-1}) was injected at the rear of the flow tube and served as the bulk flow. The gases necessary to generate the OH radicals were introduced through a 20 cm long, 1.25 cm inner diameter side arm. The organic hydroxynitrate compounds – which were added by flowing He gas through traps containing the liquid phase of the various species because of their low vapor pressures – and the competitor species (compounds used in the relative determination of OH reaction rate constants) were introduced together through a moveable injector with a fan-shaped Teflon device placed at the end to enhance mixing. All gas flow rates were monitored using calibrated mass flow meters. The ^{210}Po α-emitting ionization source was placed between the flow tube and the inlet to the CIMS. O_2 gas (99.99 %) at a flow of 6.5 STP L min^{-1} was passed through the ^{210}Po α-emitting ionization source to produce reagent ions. Pressure in the flow tube was monitored using a 0–1000 torr capacitance manometer, while temperature was measured with Cu-constantan thermocouples and held at 298 ± 2 K for most of the experiments. Most of the flow tube gases were removed at the CIMS inlet using a 31 L s^{-1} roughing pump. The pressure in the flow tube apparatus was controlled by adjusting the roughing pump valve opening.

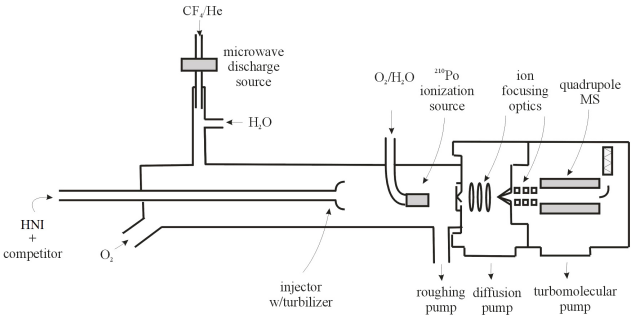

Figure 1. Schematic of the FT-CIMS apparatus. The experimental setup in this diagram shows a relative rate experiment using the $F + H_2O$ OH radical source.

2.4.2 OH source

For the present study, OH radicals were prepared by passing a dilute mixture of carbon tetrafluoride (CF_4) in He through a microwave discharge produced by a Beenakker cavity operating at 50 W. This microwave discharge-initiated dissociation of CF_4, followed by reaction with H_2O, leads to the production of OH radicals:

$$CF_4 + h\nu \rightarrow xF + CF_{4-x}, \quad \text{(R1)}$$

$$F + H_2O \rightarrow OH + HF. \quad \text{(R2)}$$

The dilute CF_4 mixture was created by combining 4 % CF_4/He (0.50 STP mL min^{-1}) with a flow of He (99.999 %, 5.00 STP L min^{-1}). This mixture was flowed through the Beenakker cavity to produce fluorine atoms (Reaction R1). The fluorine atoms were then injected in the flow tube side arm and mixed with H_2O (produced by bubbling 12 mL min^{-1} He through a trap filled with H_2O) to produce OH radicals (Reaction R2). Because H_2O is in great excess in the side arm ($[H_2O] \sim 2 \times 10^{14}$ molecules cm^{-3}) and Reaction (R2) is very fast (1.4×10^{-11} cm^3 molecule^{-1} s^{-1}) (Atkinson et al., 2007), the OH-producing reaction has a very short lifetime of about 0.4 ms, ensuring all fluorine atoms are quickly consumed. For similar experimental conditions, we have estimated that this source leads to a maximum OH radical concentration of $\sim 5 \times 10^{11}$ molecules cm^{-3} (Elrod, 2011).

2.4.3 CIMS detection

The chemical ionization reagent ions in this study were produced using a commercial ^{210}Po α-emitting source consisting of a hollow, cylindrical (69×12.7 mm) aluminium body with 10 mCi (3.7×10^8 disintegrations s^{-1}) of ^{210}Po coated on the interior walls. All oxygenated organic species were detected using a proton transfer CIMS (PTR-CIMS) scheme. Protonated water clusters were used as the reagent ion to transfer a proton to the oxygenated acceptor, M:

$$H^+(H_2O)_n + M \rightarrow MH^+(H_2O)_{n-m} + m(H_2O). \quad \text{(R3)}$$

The $H^+(H_2O)_n$ ions were produced by passing a large O_2 flow (6.5 STP L min^{-1}) through the ionization source, with H_2O impurities being sufficiently abundant to produce an adequate amount of reagent ions. The dominant chemical reagent ion was $H^+(H_2O)_4$, and the predominant proton transfer species detected were the protonated (and partially hydrated) analogues of the neutral precursor oxygenated compound. For both the OH rate constant and product studies, all ions ($MH^+(H_2O)_n$) assigned to a particular species (M) were summed and normalized to the total reagent ion signal ($H^+(H_2O)_n$) for that particular experiment in order to determine a CIMS signal that was not dependent on the ion hydrate distribution or the total ion signal.

2.4.4 OH rate constant measurement

A relative rate constant measurement similar to a recent study reported by our laboratory (Jacobs et al., 2013) was performed to measure the 4,3-HNI + OH rate constant. In this method, 4,3-HNI and a competitor with a known rate constant are flowed together through the moveable injector (described in Sect. 2.4.1) and react with the OH radical in the flow tube. Assuming both compounds react only with OH radicals under the experimental conditions, the two compounds are competing with each other for reaction with OH radicals:

$$\text{4,3-HNI} + \text{OH} \rightarrow \text{Products}, \quad \text{(R4)}$$

$$\text{Competitor} + \text{OH} \rightarrow \text{Products}. \quad \text{(R5)}$$

The rate laws for 4,3-HNI and the competitor are given by Eqs. (1)–(2), respectively:

$$\frac{\mathrm{d}[4,3-\mathrm{HNI}]}{\mathrm{d}t} = k_4[4,3-\mathrm{HNI}][\mathrm{OH}], \quad (1)$$

$$\frac{\mathrm{d}[\mathrm{Competitor}]}{\mathrm{d}t} = k_5\left[\mathrm{Competitor}\right][\mathrm{OH}], \quad (2)$$

where k_4 and k_5 are rate constants for Reactions (4) and (5), respectively. By dividing Eq. (1) by Eq. (2) and solving the resulting differential equation by separation of variables, it can be shown that

$$\ln\frac{[4,3-\mathrm{HNI}]_{t,0}}{[4,3-\mathrm{HNI}]_{t,\mathrm{OH}}} = \frac{k_4}{k_5}\ln\frac{[\mathrm{Competitor}]_{t,0}}{[\mathrm{Competitor}]_{t,\mathrm{OH}}}, \quad (3)$$

where $[4,3\text{-HNI}]_{t,0}$ and $[\text{competitor}]_{t,0}$ are the concentration of 4,3-HNI and the competitor species in the absence of OH radicals at time t, and $[4,3\text{-HNI}]_{t,\mathrm{OH}}$ and $[\text{competitor}]_{t,\mathrm{OH}}$ are the concentrations of 4,3-HNI and the competitor species in the presence of OH radicals at time t. The relative depletions of 4,3-HNI and the competitor were monitored when the OH source was turned on and off. From the relative depletions, the 4,3-HNI OH radical rate constant (k_4) was determined by plotting $\ln([4,3\text{-HNI}]_{t,0}/[4,3\text{-HNI}]_{t,\mathrm{OH}})$ vs. $\ln([\text{competitor}]_{t,0}/[\text{competitor}]_{t,\mathrm{OH}})$ and determining the slope (k_4/k_5). Because the competitor's OH radical rate constant (k_5) was known, a value for k_4 was determined.

The relative rate measurement does not require knowledge of the absolute concentrations of the epoxide and competitor species (rather, relative concentrations – which are assumed to be proportional to the CIMS signal – are required), nor does it require knowledge of the absolute reaction time (which is a fixed quantity in Eq. 3). Both of these characteristics are important for the present experiments because the vapor pressure (which is needed to calculate the absolute concentrations in the flow tube) of 4,3-HNI is unknown, and the flow tube was operated in the laminar-turbulent flow transition region (Seeley et al., 1993) where a straightforward relationship between bulk flow velocity and molecular velocities does not exist (i.e., time of reaction was not known). By operating the flow system in this transition region, the reaction time was increased and more extensive loss of both 4,3-HNI and the competitor species was observed. Different reaction conditions were obtained by varying the time of reaction (injector distance), 4,3-HNI concentration and competitor concentration. Both 4,3-HNI and the competitors contained hydroxyl groups (which are excellent proton transfer targets) and were detected using PTR-CIMS.

To assess the potential existence of systematic error, relative rate measurements for 4,3-HNI were performed using multiple competitors with varying, well-measured OH rate constants. The competitors used were methacrolein, allyl alcohol and 2-methyl-2-propen-1-ol with OH rate constants of 2.9×10^{-11} (Atkinson et al., 2006), 4.9×10^{-11} (Holloway et al., 2005; Orlando et al., 2001; Le Person et al., 2009) and 9.2×10^{-11} (Cometto et al., 2008) $\mathrm{cm^3\,molecule^{-1}\,s^{-1}}$, respectively. Using a previously described procedure (Jacobs et al., 2013), the relative depletion for each competitor was normalized to the depletion of methacrolein, and all of the data were used to determine a single value for k_4/k_5.

2.4.5 OH oxidation product study

To explore the mechanism of the OH reaction with 4,3-HNI, a PTR-CIMS-based study of the reaction products was performed. The organic hydroxynitrates were added to the flow system, and mass spectra were collected with the OH source on and off. Comparison of these mass spectra revealed which masses corresponded to products of the OH reaction. These masses were quantitatively monitored with the OH source on and off in both low-NO_x (no extra NO added) and high-NO_x (NO added to $>1\times10^{13}$ molecules $\mathrm{cm^{-3}}$) conditions. In the low-NO_x experiments, observed products are likely formed from peroxy + peroxy (including hydroperoxy formed from side reactions in the microwave OH radical source) radical interactions; while in the high-NO_x experiments, product formation is most likely from peroxy + NO reactions. Assuming equivalent PTR-CIMS response factors (each species contains an OH functional group, and previous work has shown that a variety of alcohols possess very

similar PTR rate constants; Zhao and Zhang, 2004), the relative product ratios were determined by comparing the signal from one product to the sum of the product signals. From the m/z ratios, chemical structures were assigned, and a mechanism was produced to rationalize the observed products. Different isomeric species with the same m/z ratio cannot be distinguished with this quadrupole-based CIMS instrument; therefore the proposed products are those that are easiest to rationalize in the context of the proposed mechanism and the experimental conditions. For the case of isoprene epoxide (IEPOX) formation, synthesized IEPOX was added to the flow system to confirm the IEPOX PTR-CIMS ion distribution in the matrix of the 4,3-HNI oxidation system. The pressure dependence of product formation was investigated by varying the pressure in the flow system from 50 to 400 torr by adjusting the inlet to the roughing pump. Due to the pressure-dependent efficiency of the microwave discharge source, measurements could not be performed at pressures greater than 400 torr. At the experimental pressures and timescales, it has also been shown that the flow tube acts as a nearly wall-less reactor (Seeley et al., 1993), which helps to ensure that the measured relative gas phase concentrations are representative of the true relative product yields. Nonetheless, the flow tube was also coated with halocarbon wax to further reduce gas–wall interactions, and care was taken to ensure that product signals were fully equilibrated at each point in the measurement.

2.5 Computational thermodynamics

2.5.1 Bond dissociation energy

Bond dissociation energies were theoretically determined by calculating the relative energies of the relevant species before and after a homolytic bond cleavage using an adapted version of the G2MS compound method (MG2MS) (Froese et al., 1997), a variation on Gaussian-2 (G2) theory (Curtiss et al., 1991). All calculations were carried out with the Gaussian 03 computational suite (Frisch et al., 2004), and each stationary point was confirmed as an energy minimum by inspecting the calculated frequencies. Geometries of the relevant species were optimized at the B3LYP/6–31G(d,p) level. To calculate the overall energy of the optimized structure, a base energy calculation was performed at the CCSD(T)/6–31G(d) level. In order to correct for basis set effects, a series of additive corrections were performed to simulate a CCSD(T)/6311+G(2df,2p) level calculation. The overall energy expression for the MG2MS scheme is defined as follows:

$$E_{\mathrm{MG2MS}} = E_{\mathrm{CCSD(T)/6-31G(d)}} + E_{\mathrm{MP2/6-311+G(2df,2p)}} - E_{\mathrm{MP2/6-31G(d)}} + \mathrm{HLC}, \quad (4)$$

where HLC is an empirically defined correction term with $\mathrm{HLC} = An_\alpha + Bn_\beta$, where n_α and n_β are the number of α and β electrons, respectively, and the constants A and B are 6.06 and 0.19 mH, respectively. Previous MG2MS results for atmospherically relevant systems from our lab indicate that the calculated thermodynamic properties are typically accurate to within 2.5 kcal mol^{-1} (Cappa and Elrod, 2001).

2.5.2 IEPOX-4 formation from 4,3-HNI + OH reaction coordinate calculations

The optimized structures and relative energies of the reactants, intermediates and products for IEPOX-4 (trans-β-IEPOX) formation from 4,3-HNI and BEPOX (a butane-derived epoxide) formation from 1,2-HNB were theoretically determined. In order to achieve convergence, a restricted open-shell density functional theory method was used for each single point energy calculation (ROB3LYP/6–31(d)). All calculations were carried out with the Gaussian 03 computational suite (Frisch et al., 2004). The frequencies were inspected to ensure each single point calculation was an energy minimum (or had an imaginary frequency for the transition state calculation). Reaction coordinate calculations for the 4,3-HNI mechanism were compared to those from the isoprene-derived hydroperoxide calculations previously published (Paulot et al., 2009b).

3 Results and discussion

3.1 NMR assignments

The complete NMR assignments of the synthesized hydroxynitrates are provided in the Supplement.

3.2 Hydrolysis kinetics of hydroxynitrates

The hydrolysis of the hydroxynitrate isomers was monitored in a variety of acid concentrations (0 to 2 M $HClO_4$), and, regardless of the acid concentration, the rate of hydrolysis remained constant. Thus, a general acid-catalyzed mechanism (where water protonates the bridging oxygen atom on the nitrate) was assumed to be the predominant hydrolysis mechanism (Whalen, 2005). A standard first-order analysis of hydroxynitrate depletion was performed for each hydrolysis reaction. Figure 2 provides a sample plot of $\ln([\mathrm{HNI}]/[\mathrm{HNI}]_0)$ as a function of time for the reaction of 4,3-HNI in D_2O using the relative integrated areas of the methyl group protons in 4,3-HNI and the diol products in ^{1}H NMR spectra to calculate $[4,3\text{-HNI}]/[4,3\text{-HNI}]_0$. The slope from this linear regression is equal to $-k$, the neutral solution hydrolysis rate constant. A similar procedure was used for 1,4-HNI hydrolysis, but (because of product and reactant peak overlap in the methyl region) DSS was added to the reaction mixture and depletion of the hydroxynitrate relative to the peak at 0.00 ppm was monitored. Because of the overlap problem, hydrolysis kinetics of the specific E and Z 1,4-HNI isomers were unable to be distinguished, and a generic 1,4-HNI hydrolysis rate was measured.

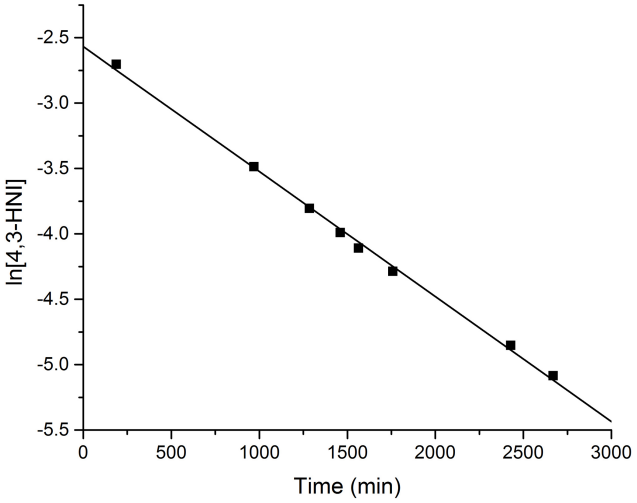

Figure 2. Sample first-order reactant kinetics plot for the hydrolysis of 4,3-HNI under (initially) neutral D_2O conditions.

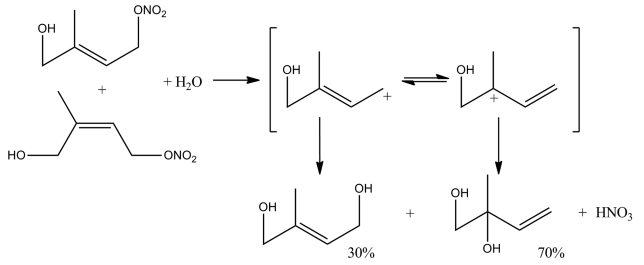

Figure 3. Mechanism for 1,4-HNI hydrolysis with the distribution of products observed.

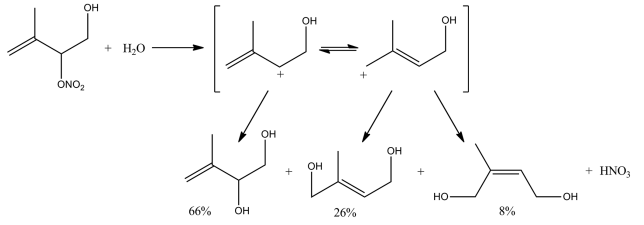

Figure 4. Mechanism for 4,3-HNI hydrolysis with the distribution of products observed.

The mechanism and distribution of products observed for 1,4-HNI and 4,3-HNI hydrolysis are given in Figs. 3 and 4, respectively. In aqueous solution, 1,4-HNI and 4,3-HNI were found to have first-order hydrolysis rate constants of $(6.76 \pm 0.09) \times 10^{-3}\,s^{-1}$ and $(1.59 \pm 0.03) \times 10^{-5}\,s^{-1}$, respectively. These hydrolysis rate constants indicate that the 1,4-HNI and 4,3-HNI lifetimes in neutral solution are 2.46 min and 17.5 h, respectively. The hydrolysis rate constants of similar isoprene-derived, saturated hydroxynitrates have previously been measured in our lab (Darer et al., 2011; Hu et al., 2011). The saturated primary nitrates were found to have lifetimes > 2500 h, while the saturated tertiary nitrates had lifetimes of a few minutes in neutral solution. Thus the allylic nature of the 1,4-HNI and 4,3-HNI transition states apparently lowers the activation barrier sufficiently to make neutral hydrolysis of the primary and secondary hydroxynitrates occur on a much faster timescale than the previously studied saturated primary and secondary hydroxynitrates of isoprene. This hypothesis was tested by measuring the hydrolysis rate constant for another allylic, non-isoprene-derived hydroxynitrate, 1,2-HNB. The hydrolysis rate constant and neutral solution lifetime were $(9.95 \pm 0.30) \times 10^{-6}\,s^{-1}$ and 28 h, respectively. The hydrolysis reaction for the unsaturated species was again faster than that of similar saturated species, presumably because of the resonance stabilized carbocation.

The products were identified using ^{1}H NMR after the hydrolysis reactions had run to completion (> 3 lifetimes). Each of the diol products had been previously prepared in our lab, and NMR spectra of each were available for reference. Quantification of the product distribution was accomplished using the integrated areas of the peaks in the methyl region. Based on the distribution of products, it appears that (as expected) the dominant product for both of the isomers is derived from the more substituted carbocation intermediate. For 1,4-HNI hydrolysis, 70 % of the product is derived from the tertiary carbocation, with the remaining 30 % being derived from the primary carbocation. The yields for 4,3-HNI hydrolysis were similar, with the secondary carbocation leading to 66 % of the total product and the primary carbocation leading to 34 % of the total product. The "E" primary carbocation diol was preferred in both cases; it formed 100 % of the time for the 1,4-HNI product (even though the initial product was 5 : 1 E : Z 1,4-HNI) and was preferred in a 3 : 1 ratio over the Z isomer for the 4,3-HNI hydrolysis.

3.3 Gas phase oxidation of hydroxynitrates

While both 4,3-HNI and 1,4-HNI were successfully synthesized, only 4,3-HNI was thermally stable enough for study in our flow tube CIMS system. Presumably because of its fast hydrolysis rate constant and the presence of some water impurity, 1,4-HNI quickly decomposed into both the diol and a more volatile aldehyde. While the aldehyde component represented only a minor fraction of the condensed phase 1,4-HNI sample (as ascertained via ^{1}H NMR), the very high vapor pressure of the aldehyde led to a gas phase situation in which 1,4-HNI was a minor component.

3.3.1 Gas phase OH rate constant of 4,3-HNI

The OH rate constant for 4,3-HNI was obtained via competition experiments, using methacrolein, allyl alcohol and 2-methyl-2-propen-1-ol as the competitors with known rate constants. Like 4,3-HNI, all of the competitors were unsaturated alkenols which reacted with OH via

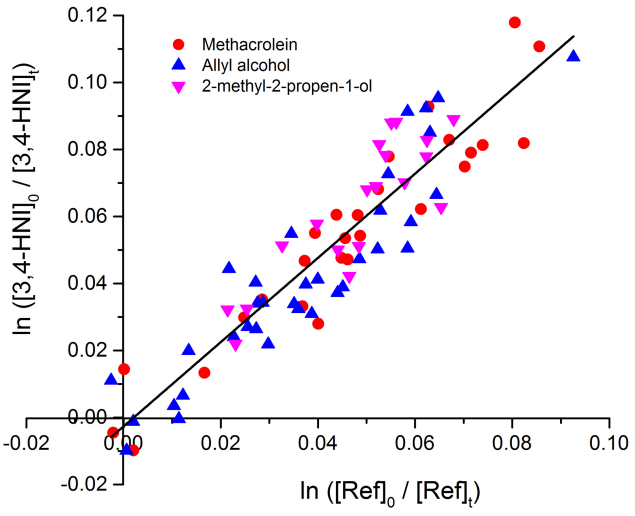

Figure 5. Relative rate constant determination for 4,3-HNI.

an addition mechanism and at the usual 100 torr operating pressure of the flow tube were all at their high pressure rate constant limit. The signals from the competitors and 4,3-HNI were monitored with the OH source on and off. Because all of the competitors were normalized to methacrolein, all of the data for each competitor were plotted together. The plot of $\ln([4,3\text{-HNI}]_{t,0}/[4,3\text{-HNI}]_{t,\mathrm{OH}})$ vs. $\ln([\text{competitor}]_{t,0}/[\text{competitor}]_{t,\mathrm{OH}})$ is shown in Fig. 5. The slope of the best fit line in Fig. 5, 1.257 ± 0.058, is equal to the ratio of 4,3-HNI's OH rate constant to methacrolein's OH rate constant (k_4/k_5). From methacrolein's OH rate constant, $2.9 \pm 0.3 \times 10^{-11}$ cm^3 molecule^{-1} s^{-1} (Atkinson et al., 2006), the 4,3-HNI + OH rate constant was calculated to be $3.64 \pm 0.41 \times 10^{-11}$ cm^3 molecule^{-1} s^{-1} (one standard deviation error, which includes contributions from both the relative rate constant uncertainty in k_4/k_5 and uncertainty in the absolute rate constant of the competitor).

A very recent study has reported the OH rate constant with 4,3-HNI and found it to be $(4.2 \pm 0.7) \times 10^{-11}$ cm^3 molecule^{-1} s^{-1} (Lee et al., 2014). This value is in good agreement with the 4,3-HNI OH rate constant measured in this work and confirms the expectation that the OH rate constant is not pressure dependent between 100 and 760 torr total pressure. The OH rate constant for a similar hydroxynitrate, 2-hydroxy-1-nitrato-but-3-ene (2,1-HNB), was measured separately and found to be $(3.62 \pm 0.72) \times 10^{-11}$ cm^3 molecule^{-1} s^{-1} (Treves and Rudich, 2003). Therefore, it appears that the value of the OH + 4,3-HNI rate is well constrained by several experimental measurements.

3.3.2 4,3-HNI gas phase oxidation product study

Identification of products

Because 4,3-HNI is an unsaturated hydrocarbon, it is expected to react with OH via an addition mechanism forming a hydroxy alkyl radical. The OH radical could add to either of the carbon atoms in the double bond, so there is the potential for multiple, different reaction pathways. As described in the experimental section, the product species were identified by comparing mass spectra taken with the microwave on and off, and then looking for new signals in the "OH-source-on" PTR-CIMS spectrum. Because all of the predicted products contained alcohol groups, they were all assumed to have equal PTR-CIMS response factors. This allowed direct comparison of the signals to determine the relative molar product yields.

Table 2 shows the deduced product structure (based on the $MH^+(H_2O)_n$ signal carriers observed), with the specific isomers rationalized within the context of the overall mechanism. For the cases of C–C bond dissociation reaction types, there are two reaction products. However, due to mass coincidence complications, only one of the products (the product listed in Table 2) was quantified via PTR-CIMS in each case. From the structures of the products, a proposed mechanism for the formation of products from 4,3-HNI was developed (Fig. 6). Based on the products observed, it seems likely that the OH radical adds to the double bond almost exclusively at the C1 position. This generates the thermodynamically preferred tertiary radical over the primary radical from C2 addition. The alkyl radical can either undergo a unimolecular rearrangement to produce an IEPOX – either cis- or trans-β-IEPOX (IEPOX-3 and IEPOX-4, respectively) – and NO_2, or it can react with O_2, forming a peroxy radical. The competition between the two reactions was found to be pressure dependent and is discussed below. The peroxy radical can react with either NO (added to the flow system) or HO_2 (a by-product of the microwave discharge source) to generate the alkoxy radical. The C2–C3 bond can fission, generating hydroxyacetone (HAC), glycolaldehyde and NO_2, or the C1–C2 bond can break, which results in formaldehyde and a methyl vinyl ketone hydroxy nitrate (MVKN). The relative yields of the products observed by PTR-CIMS at 50 and 760 torr (based on the analysis described below) are given in Table 2.

IEPOX was identified as a major product at the lower pressure conditions by its unique PTR-CIMS ion distribution. Previous work in our laboratory investigated the reaction of IEPOX with the OH radical (Jacobs et al., 2013), and thus mass spectra of previously collected IEPOX (as well as a sample of previously synthesized IEPOX) were on hand and aided in the identification of IEPOX. In the previous work, PTR-CIMS of IEPOX had peaks at m/z 101, 137, 155, 219 and 237, which represent (IEPOX)H^+-H_2O, (IEPOX)$(H_2O)H^+$, (IEPOX)$(H_2O)_2H^+$, (IEPOX)$_2H^+$-H_2O

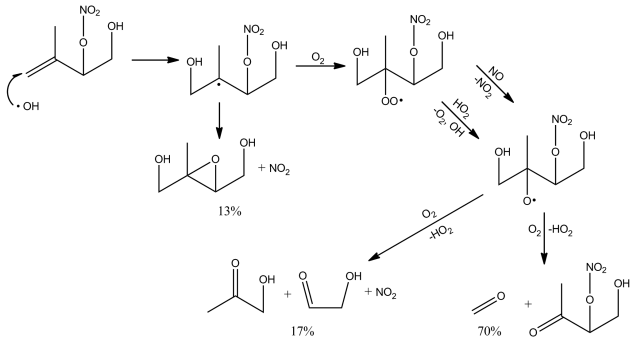

Figure 6. Gas phase OH-initiated oxidation mechanism for 4,3-HNI (calculated 760 torr relative yields are given).

Table 2. Relative product yields for 4,3-HNI oxidation at 50 torr (experimental) and 760 torr (calculated).

m/z (MH^+)	Deduced molecular species	Relative yield 50 torr (%)	Relative yield 760 torr (%)
75	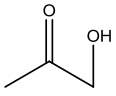	10	17
119	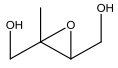	71	13
150	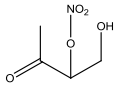	19	70

and $(IEPOX)_2H^+$, respectively. All five of these product peaks were observed in the 4,3-HNI product spectra. To confirm there were no matrix effects at work in the 4,3-HNI product studies, the previously synthesized IEPOX was added downstream of the OH source (where it would not have a chance to react with OH radicals), and all of the peaks attributed to IEPOX increased as expected. Thermodynamic calculations for IEPOX formation from 4,3-HNI were performed and compared to the previously proposed mechanism for IEPOX formation from hydroxy peroxides (Paulot et al., 2009b) to further support the experimental observations.

A previous atmospheric chamber study looking at the oxidation of 4,3-HNI by the OH radical has also proposed a reaction mechanism (Lee et al., 2014). This reaction mechanism, derived from experiments performed very near atmospheric pressure, also includes MVKN-forming (C1–C2 bond-breaking) and hydroxyacetone-forming (C3–C4 bond-breaking) channels with 72 and 10 % yields, respectively. Their mechanism also suggests that < 18 % of 4,3-HNI forms a dinitrate species. Unlike the present work, the Lee et al. mechanism does not include IEPOX formation from 4,3-HNI. Our experimental results show that (at atmospheric pressure) the MVKN-forming channel, the hydroxyacetone/NO_2-forming channel and the IEPOX/NO_2-forming channel account for 70, 17 and 13 % of the total product yield, respectively. Many of the aspects in our mechanism coincide with the mechanism proposed by Lee et al. (2014) with the exception of a minor, but significant, IEPOX-producing product channel.

Product pressure dependence

At higher pressures the relative yield of IEPOX from 4,3-HNI decreased. This observation was explained by assuming that the OH + 4,3-HNI reaction followed a Lindemann–Hinshelwood-type mechanism (i.e., the energized OH-4,3-HNI adduct can revert to OH + 4,3-HNI, be de-energized by collision or go on to form products):

$$4,3-\mathrm{HNI}+\mathrm{OH}\rightarrow 4,3-\mathrm{HNI}-\mathrm{OH}^*, \quad \text{(R6)}$$

$$4,3-\mathrm{HNI}-\mathrm{OH}^*\rightarrow 4,3-\mathrm{HNI}+\mathrm{OH}, \quad \text{(R7)}$$

$$4,3-\mathrm{HNI}-\mathrm{OH}^*+\mathrm{M}\rightarrow 4,3-\mathrm{HNI}-\mathrm{OH}+\mathrm{M}^*, \quad \text{(R8)}$$

$$4,3-\mathrm{HNI}-\mathrm{OH}^*\rightarrow \mathrm{IEPOX}+\mathrm{NO_2}, \quad \text{(R9)}$$

$$4,3-\mathrm{HNI}-\mathrm{OH}^*+\mathrm{M}\rightarrow \mathrm{Otherproducts}+\mathrm{M}^*, \quad \text{(R10)}$$

where * represents a high-energy complex. At low pressures (low [M]), Reaction (R6) competes with Reaction (R7), and the activated complex can revert back to reactants. Previous research has shown that isoprene's OH rate constant does not change between 2 and 6 torr, indicating that isoprene is at its high-pressure limit at 2 torr (Chuong and Stevens, 2000). The relatively low threshold for the high-pressure limit was attributed to the isoprene complex's ability to distribute energy into many vibrational modes and thus decrease the energy in the critical CO vibration. Because 4,3-HNI is an even larger molecule than isoprene and has even more vibrational modes, the relative rate of Reaction (R7) as compared to Reaction (R8) is expected to be even more insignificant at the experimental pressures (> 50 torr).

However, because Reaction (R8) is dependent on the number of total gas molecules present (i.e., pressure), and the rate of IEPOX formation was observed to decrease at higher pressures, it was assumed that IEPOX was formed from the 4,3-HNI-OH* activated complex. Thus, the alkyl radical branching point in Fig. 6 can be more accurately represented by the two competing reactions, Reactions (R9) and (R10). The IEPOX and "other products" (OP) rates of formation can then be defined as follows:

$$\frac{\mathrm{d[IEPOX]}}{\mathrm{d}t}=k_9[4,3-\mathrm{HNI}-\mathrm{OH}^*], \quad (5)$$

$$\frac{\mathrm{d[OP]}}{\mathrm{d}t}=k_{10}[\mathrm{M}][4,3-\mathrm{HNI}-\mathrm{OH}^*], \quad (6)$$

where k_9 and k_{10} are the rates of Reactions (R9) and (R10), respectively. Combining these two expressions yields an equation for the rate of total product (TP) formation:

$$\frac{\mathrm{d[TP]}}{\mathrm{d}t}=k_9\left[4,3-\mathrm{HNI}-\mathrm{OH}^*\right]+k_{10}[\mathrm{M}][4,3-\mathrm{HNI}-\mathrm{OH}^*]. \quad (7)$$

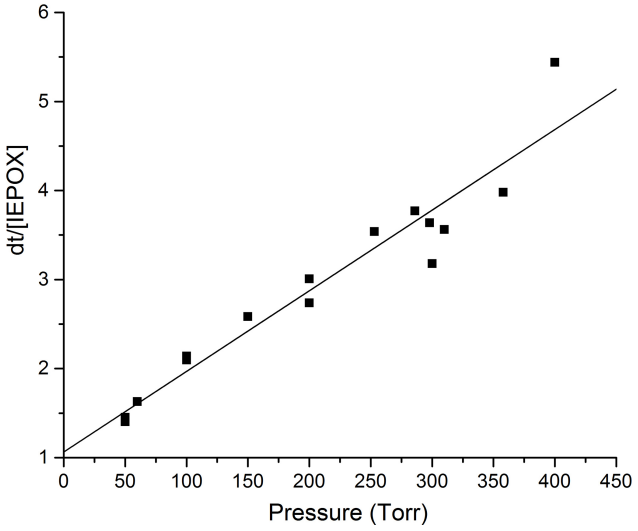

Figure 7. Pressure dependence of the inverse relative IEPOX yield from 4,3-HNI.

The relative yield of IEPOX can then be expressed as the IEPOX rate of formation (Eq. 6) over the total product rate of formation (Eq. 7):

$$\frac{\frac{\mathrm{d[IEPOX]}}{\mathrm{d}t}}{\frac{\mathrm{d[TP]}}{\mathrm{d}t}} = \frac{\mathrm{d[IEPOX]}}{\mathrm{d[TP]}} = \frac{k_9[4,3-\mathrm{HNI}-\mathrm{OH}^*]}{k_9\left[4,3-\mathrm{HNI}-\mathrm{OH}^*\right] + k_{10}[\mathrm{M}]\left[4,3-\mathrm{HNI}-\mathrm{OH}^*\right]} = \frac{k_9}{k_9 + k_{10}[\mathrm{M}]}. \quad (8)$$

Taking the reciprocal of Eq. (8) yields an expression that is linearly dependent on [M] (and thus pressure):

$$\frac{\mathrm{d[TP]}}{\mathrm{d[IEPOX]}} = \frac{k_9 + k_{10}[\mathrm{M}]}{k_9}\,\alpha\,1 + \frac{k_{10}}{k_9}P. \quad (9)$$

By plotting the inverse of the relative yield of IEPOX vs. pressure, a linear relationship was determined that was used to estimate the relative yield of IEPOX at atmospheric pressure (Fig. 7). The slope of the best fit line in Fig. 7, $y = [(9.05 \pm 0.73) \times 10^{-3}]\ P(\mathrm{torr}) + 1.07 \pm 0.17$, was used to estimate the yield of IEPOX from 4,3-HNI at atmospheric pressure presented in Table 2. The relative error from the linear regression propagated into the calculated atmospheric pressure IEPOX relative yield was less than 0.08 (13 ± 1 %). When extrapolated to lower pressures (0 torr), the yield of IEPOX is calculated to approach 100 %, as predicted by Eq. (9). Taken together, these characteristics of the regression analysis demonstrate that the pressure dependence findings are well described by our model. Over each of the entire measured pressure range (50–400 torr), on average the ratio of MVKN formation to HAC formation was observed to remain constant (4.01 ± 0.98). The yields of these two channels at atmospheric pressure were determined by using this ratio and the calculated relative yield of IEPOX. All of the extrapolated relative yields are given in Table 2.

Table 3. Relative product yields for 1,2-HNB oxidation at 50 torr (experimental) and 760 torr (calculated).

m/z (MH^+)	Deduced molecular species	Relative yield 50 torr (%)	Relative yield 760 torr (%)
61		3	12
105	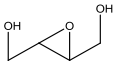	86	16
136	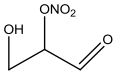	11	71

3.3.3 1,2-HNB gas phase oxidation product study

To assess the feasibility of IEPOX formation from other currently synthetically inaccessible isoprene-derived hydroxynitrates, a gas phase oxidation product study on 1,2-HNB was performed to see if epoxide products were formed. The relative yields of the observed products and a proposed mechanism for the formation of the observed products are provided in Table 3 and Fig. 8, respectively. The mechanism is similar to that of 4,3-HNI: the OH radical initially adds to carbon 4, creating a secondary alkyl radical. The radical can then undergo unimolecular rearrangement to form a butane epoxide (BEPOX) and NO_2, or it can react with O_2, forming the peroxy radical. The peroxy radical reacts with either NO or HO_2 to create the alkoxy radical. Reaction with O_2 can cause the C3–C4 bond to break, resulting in formaldehyde and hydroxynitrate propanal, or the C2–C3 bond can break, leading to two equivalents of glycolaldehyde and the release of one NO_2 molecule. The proportion of C3–C4 to C2–C3 bond fragmentation in 1,2-HNB oxidation is roughly the same as the proportion of C1–C2 to C2–C3 bond fragmentation in 4,3-HNI oxidation. Thus, 1,2-HNB and 4,3-HNI release roughly the same amount of NO_2 when further oxidized by OH.

At higher pressures, the relative epoxide yields were once again observed to decrease. The mechanism for BEPOX formation from 1,2-HNB was assumed to be the same as the mechanism for IEPOX formation from 4,3-HNI, and a pressure dependence product study was performed. Again the inverse of the relative yield of BEPOX was plotted vs. pressure to give a linear relationship (Fig. 9). The slope of the best fit line in Fig. 9, $y = [(6.80 \pm 0.44) \times 10^{-3}]\ P(\mathrm{torr}) + 0.89 \pm 0.09$, was used to estimate the yield of BEPOX from 1,2-HNB at atmospheric pressure presented in Fig. 8. The ratio of C3–C4 bond splitting and C2–C3 bond splitting products was found to be constant, on average, throughout the experiment (5.8 ± 1.6). This ratio (with the calculated relative yield of BEPOX) was used to determine

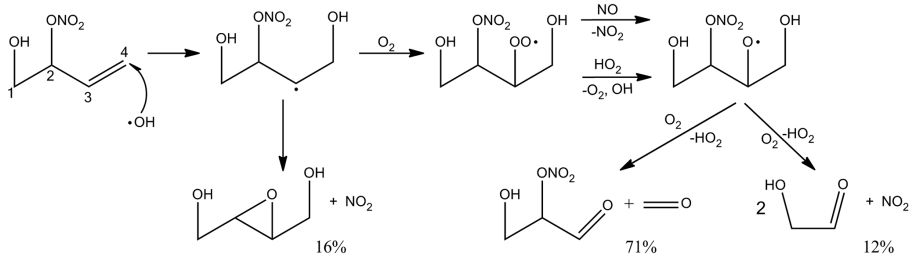

Figure 8. Gas phase OH-initiated oxidation mechanism for 1,2-HNB (calculated 760 torr relative yields are provided).

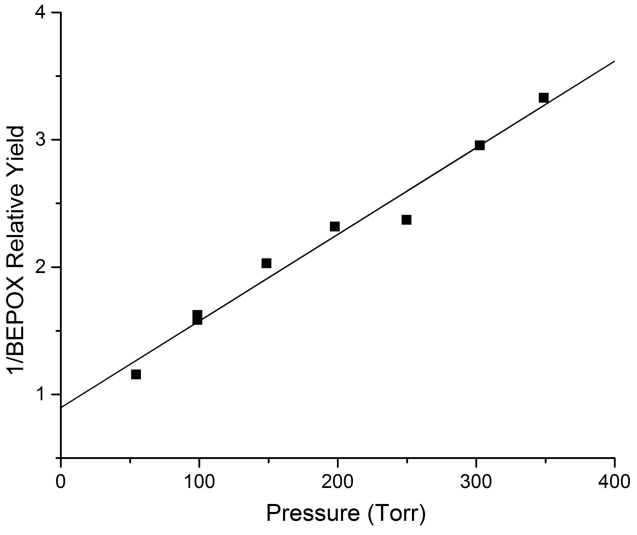

Figure 9. Pressure dependence of the inverse relative BEPOX yield from 1,2-HNB.

the yields of the fragmentation pathways at atmospheric pressure. The calculated relative yields of the products at atmospheric pressure are presented in Table 3 and Fig. 8.

The formation of IEPOX from 4,3-HNI and BEPOX from 1,2-HNB suggests that epoxide formation may be a general mechanism that is operative whenever an alkyl radical is adjacent to the nitrate functional group. This finding suggests that other isomers of isoprene-derived hydroxynitrates should be capable of forming IEPOX compounds through OH reaction.

3.4 IEPOX formation thermodynamics calculations

3.4.1 Bond dissociation energy calculations

To confirm the feasibility of IEPOX (specifically IEPOX-4 or trans-β-IEPOX) formation from 4,3-HNI, the O–N bond dissociation energy was calculated and compared to the O–O bond dissociation energy for isoprene hydroxyperoxide (ISOPOOH), the previously proposed IEPOX-4 precursor (Paulot et al., 2009b). The calculations were performed using the adapted G2MS procedure described in the experimental section. The energies of the relevant species were calculated according to Eq. (4), and the bond dissociation energy was determined by finding the difference in energy between the products and reactants after homolytic cleavage of the relevant bond. The O–O and O–N bond dissociation energies for hydrogen peroxide and nitric acid were also calculated, both to validate the MG2MS method and to serve as a point of comparison for the bond dissociation energies for the isoprene-derived compounds. The calculated bond dissociation energies are presented in Table 4.

The experimental O–O and O–N bond dissociation energies for hydrogen peroxide and nitric acid are 50.4 and 49.3 kcal mol^{-1}, respectively (Lou, 2007). Thus, as found in our previous implementation of the MG2MS method, the calculated values are quite accurate (Cappa et al., 2001). The O–N bond dissociation energy for 4,3-HNI is somewhat lower than the O–O bond dissociation energy for ISOPOOH. While this calculation does not rationalize the kinetic feasibility of 4,3-HNI as a precursor to IEPOX-4 formation, it does demonstrate the thermodynamic feasibility of IEPOX-4 formation from either 4,3-HNI or ISOPOOH.

3.4.2 IEPOX-4 formation from 4,3-HNI + OH reaction coordinate calculations

All stationary points in the reaction of 4,3-HNI to IEPOX-4 (trans-β-IEPOX) and in the reaction of 1,2-HNB to trans-BEPOX were optimized with the ROB3LYP/6–31G(d) method. The transition state (TS) between the alkyl radical and the epoxide each had a single imaginary frequency at 635 and 731 cm^{-1} for the 4,3-HNI and 1,2-HNB derived species, respectively. As anticipated, this imaginary mode is a vibration along the O–N bond. The single point energies for the 4,3-HNI to IEPOX-4 and 1,2-HNB to trans-BEPOX reactions are provided in Table 5, and the reaction coordinate diagram for IEPOX-4 formation is provided in Fig. 10. The previous calculations performed to rationalize IEPOX formation from ISOPOOH found that the level of theory and choice of basis sets used did not significantly influence relative energy aspects of the reaction coordinate diagram (Paulot et al., 2009b). However, we found that restricted open-shell density functional theory methods were needed to ensure that energy convergence was achieved for all species. To provide

Table 4. Calculated 0 K bond dissociation energies (D_0) for the relevant species.

Bond	O–N (4,3-HNI)	O–N ($HONO_2$)	O–O (ISOPOOH)	O–O (H_2O_2)
D_0 (kcal mol^{-1})	40.6	49.6	43.8	49.9

Table 5. Calculated relative energies (kcal mol^{-1}) of the stationary points in the reactant + OH → epoxide + NO_2 reaction. All energies were calculated using the ROB3LYP/6–31G(d) method.

Species	4,3-HNI	1,2-HNB	ISOPOOH
Reactant	0	0	0
Alkyl radical	−36.7	−32.5	−33.0
Transition state	−25.2	−21.5	−29.4
Epoxide product	−51.0	−53.3	−42.5

a comparison and corroborate our results, single point energy calculations for IEPOX-4 formation from ISOPOOH were repeated using the ROB3LYP/6–31G(d) method. The calculated energies followed the same general trend as previously observed and had an activation energy (3.6 kcal mol^{-1}) that was in good agreement with the calculations previously performed on this reaction pathway (Paulot et al., 2009b). The single point energies for the ISOPOOH reaction are also listed in Table 5.

The pressure dependence study suggests that the majority of IEPOX formation is derived from the activated 4,3-HNI-OH complex, which has the same energy as the initial reactants. Because the energy of this species far exceeds the energy of the transition state, the magnitude of the activation energy is irrelevant, as depicted in Fig. 10. However, once the complex is collisionally deactivated and the excess energy is removed, the energies of the reaction barriers become relevant again. The energy barrier between the alkyl radical and the TS was found to be higher (11.5 kcal mol^{-1}) for the 4,3-HNI pathway than the ISOPOOH pathway. Thus, once deactivated, substantially less IEPOX is expected to be produced from the 4,3-HNI alkyl radical than the ISOPOOH alkyl radical. Additionally, because the 4,3-HNI-derived alkyl radical is larger and contains more vibrational modes than the ISOPOOH-derived alkyl radical, the 4,3-HNI-OH activated complex is expected to be more easily deactivated by collision than the ISOPOOH-OH activated complex. Taken together, these findings are qualitatively consistent with the present findings that IEPOX only accounts for 13 % of the total product formed from 4,3-HNI oxidation, while the previous work measured a 75 % IEPOX yield from ISOPOOH oxidation at atmospheric pressure (Paulot et al., 2009b).

The BEPOX-forming pathway had a similar energy barrier (11.0 kcal mol^{-1}) to that of the 4,3-HNI pathway, and the 1,2-HNB-OH activated complex is expected to be collisionally deactivated in a similar manner to the 4,3-HNI-OH complex. Again this finding is qualitatively consistent with the finding that IEPOX and BEPOX have similar yields at atmospheric pressure (16 % for BEPOX compared to the 13 % for IEPOX). Because it is certainly possible for IEPOX to also form from the deactivated alkyl radical (as proposed by Paulot et al., 2009b), the atmospheric pressure yields of IEPOX calculated in this study for the 4,3-HNI + OH reaction are lower bound estimates.

4 Atmospheric implications

4.1 Potential aerosol phase hydrolysis of 4,3-HNI and 1,4-HNI

The 4,3-HNI and E / Z 1,4-HNI isomers have previously been identified as the products of OH-initiated, high-NO_x oxidation of isoprene (Lockwood et al., 2010; Paulot et al., 2009a). Additionally, Rindelaub et al. recently demonstrated that, for similar species produced from α pinene, the aerosol phase partitioning reaction was competitive with the gas phase oxidation processes (Rindelaub et al., 2014). If the Henry's law constants for 4,3-HNI and 1,4-HNI (and other isoprene-derived hydroxynitrates) are large enough, the hydrolysis constants measured in this work indicate that aerosol phase hydrolysis (at all pH values, due to the general acid catalysis mechanism) should be efficient on an atmospherically relevant timescale (< 1 day).

4.2 Gas phase OH-initiated oxidation of 4,3-HNI

The experimental determination of a fast OH + 4,3-HNI rate constant confirms the expectation that isoprene hydroxynitrates will have a relatively short atmospheric lifetime (for an average OH concentration of 1×10^6 molecules cm^{-3}, the 4,3-HNI lifetime is only 7.6 h). The observation of NO_x recycling product pathways suggests that the traditional categorization of low- and high-NO_x processes for isoprene is inadequate for the description of the actual, more subtle mechanisms at work in the atmosphere. In addition to the NO_x recycling, the present finding that a high-NO_x species, 4,3-HNI, can lead to the important "low-NO_x" species, IEPOX, emphasizes this point. Several studies have shown that IEPOX is an important isoprene intermediate for the formation of species formed in SOA formation (Paulot et al., 2009b; Cole-Filipiak et al., 2010; Darer et al., 2011; Lin et al., 2012; Surratt et al., 2010). Based on the IEPOX- and BEPOX-forming mechanisms that we have proposed from the OH + 4,3-HNI and OH + 1,2-HNB reactions, respectively, we also expect

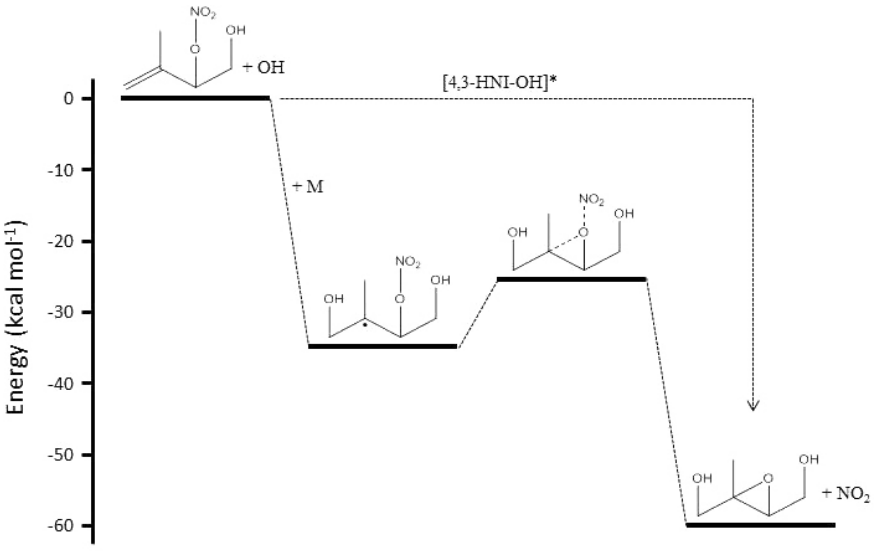

Figure 10. Relative energies for the formation of trans-IEPOX from 4,3-HNI. The activated alkyl radical (4,3-HNI-OH*) resulting from the addition of OH onto the 4,3-HNI double bond is formed with enough excess energy that it can decompose into IEPOX + NO_2 via the transition state. Only after being collisionally deactivated by another molecule (M) does the activation barrier to the TS become relevant. Energies calculated with the ROB3LYP/6–31G(d) method.

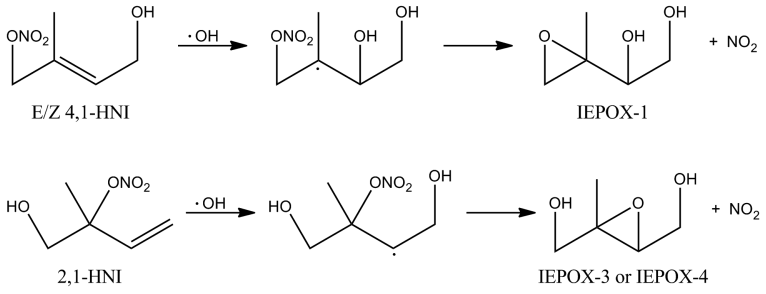

Figure 11. Proposed mechanism for IEPOX formation from 4,1-HNI and 2,1-HNI. For both hydroxynitrate isomers, the thermodynamically favored alkyl radical is adjacent to the nitrate group, potentially leading to IEPOX formation.

that the OH reactions with 1,2-HNI and both E / Z 4,1-HNI (Table 1) should also be capable of producing an IEPOX compound. These three hydroxynitrate isomers would go through an intermediate in which the alkyl radical is adjacent to the nitrate group (Fig. 11). IEPOX is also possible from E / Z 1,4-HNI, but the OH-initiated oxidation would need to lead to the secondary alkyl radical instead of the thermodynamically preferred tertiary radical. Therefore, IEPOX formation from 1,4-HNI is not likely. Based on the isomer-specific isoprene hydroxynitrate product distributions previously reported (Paulot et al., 2009a), we estimate that 65 % of isoprene hydroxynitrates have the ability to form IEPOX. The present findings indicate a potentially greater role for IEPOX even under high-NO_x atmospheric conditions, which could impact our understanding of both the gas and aerosol phase chemistry of isoprene-derived compounds for varying NO_x conditions. Indeed, this newly discovered mechanism may help to explain the previous detection of IEPOX-derived SOA components under high-NO_x conditions (Surratt et al., 2010; Budisulistiorini et al., 2013).

5 Conclusions

4-hydroxy-3-nitroxy isoprene (4,3-HNI) and E / Z 1-hydroxy-4-nitroxy isoprene (1,4-HNI), representing three of the eight possible isoprene-derived hydroxynitrates, have been synthesized and characterized with NMR. The unimolecular, neutral-solution hydrolysis rate constants for 4,3-HNI and the 1,4-HNI isomers (as determined via NMR spectroscopy) were $(1.59 \pm 0.03) \times 10^{-5}\,s^{-1}$ and $(6.76 \pm 0.09) \times 10^{-3}\,s^{-1}$, respectively. The measured rate constants were unaffected by increasing acid strength (up to 2.0 M $HClO_4$); thus a general acid catalysis mechanism (where water molecules protonate the bridging oxygen atom) was proposed. The lifetimes of these unsaturated

hydroxynitrates (17.5 h and 2.46 min for 4,3-HNI and 1,4-HNI, respectively) are several orders of magnitude smaller than the lifetimes for similar non-tertiary saturated hydroxynitrates.

The rate constant for the OH-radical-initiated oxidation of 4,3-HNI was measured using the FT-CIMS relative rate technique. The OH rate constant was measured to be $(3.64 \pm 0.41) \times 10^{-11}$ cm^3 molecule^{-1} s^{-1}. A mechanism for the formation of the observed products (including an IEPOX species) was proposed (Fig. 6). Based on estimates of the atmospheric pressure yields of the products, roughly 30 % of the NO_x sequestered by 4,3-HNI will be released upon OH reaction. IEPOX, a species important for SOA formation, was observed to be a minor but significant product of 4,3-HNI oxidation. This new IEPOX-forming pathway was supported by computational results that indicate that the reaction mechanism is similar to the established hydroperoxide IEPOX-forming pathway (Paulot et al., 2009b). A similar experimental and computational investigation of the OH reaction with 1-hydroxy-2-nitroxy-3-butene (1,2-HNB) also indicated significant epoxide product formation. Based on these findings, it is expected that several of the other isoprene-derived hydroxynitrates, in total accounting for 65 % of all isoprene-derived hydroxynitrates, will also be able to form IEPOX species. The formation of IEPOX (a low-NO_x compound) from a hydroxynitrate (a high-NO_x compound) suggests that, as has previously been discussed (Wennberg, 2013), the traditional low- and high-NO_x descriptors are insufficient to explain the more subtle chemical mechanisms at work in the atmosphere.

The Supplement related to this article is available online at doi:10.5194/acp-14-8933-2014-supplement.

Acknowledgements. This work was supported by the National Science Foundation under grant no. 1153861.

Edited by: V. F. McNeill

References

Atkinson, R.: Gas-phase tropospheric chemistry of organic compounds: a review, Atmos. Environ., 24, 1–41, 1990.

Atkinson, R., Baulch, D. L., Cox, R. A., Crowley, J. N., Hampson, R. F., Hynes, R. G., Jenkin, M. E., Rossi, M. J., Troe, J., and IUPAC Subcommittee: Evaluated kinetic and photochemical data for atmospheric chemistry: Volume II – gas phase reactions of organic species, Atmos. Chem. Phys., 6, 3625–4055, doi:10.5194/acp-6-3625-2006, 2006.

Atkinson, R., Baulch, D. L., Cox, R. A., Crowley, J. N., Hampson, R. F., Hynes, R. G., Jenkin, M. E., Rossi, M. J., and Troe, J.: Evaluated kinetic and photochemical data for atmospheric chemistry: Volume III – gas phase reactions of inorganic halogens, Atmos. Chem. Phys., 7, 981–1191, doi:10.5194/acp-7-981-2007, 2007.

Budisulistiorini, S. H., Canagaratna, M. R., Croteau, P. L., Marth, W. J., Baumann, K., Edgerton, E. S., Shaw, S. L., Knipping, E. M., Worsnop, D. R., Jayne, J. T., Gold, A., and Surratt, J. D.: Real-yime continuous characterization of secondary organic aerosol derived from isoprene epoxydiols in downtown Atlanta, Georgia, using the Aerodyne Aerosol Chemical Speciation Monitor, Environ. Sci. Technol., 47, 5686–5694, doi:10.1021/es400023n, 2013.

Cappa, C. D. and Elrod, M. J.: A Computational Investigation of the Electron Affinity of CO_3 and the Thermodynamic Feasibility of $CO_3^-(H_2O)_n$ + ROOH Reactions, Phys. Chem. Chem. Phys., 3, 2986–2694, 2001.

Carlton, A. G., Wiedinmyer, C., and Kroll, J. H.: A review of Secondary Organic Aerosol (SOA) formation from isoprene, Atmos. Chem. Phys., 9, 4987–5005, doi:10.5194/acp-9-4987-2009, 2009.

Chen, X., Hulbert, D., and Shepson, P. B.: Measurement of the organic nitrate yield from OH reaction with isoprene, J. Geophys. Res., 103, 25563–25568, doi:10.1029/98JD01483, 1998.

Chuong, B. and Stevens, P. S.: Kinetic Study of the OH + Isoprene and OH + Ethylene Reactions between 2 and 6 Torr and over the Temperature Range 300–423 K, J. Phys. Chem. A, 104, 5230–5237, 2000.

Chuong, B. and Stevens, P. S.: Measurements of the kinetics of the OH-initiated oxidation of isoprene, J. Geophys. Res., 107, 4162, doi:10.1029/2001JD000865, 2002.

Cole-Filipiak, N. C., O'Connor, A. E., and Elrod, M. J.: Kinetics of the hydrolysis of atmospherically relevant isoprene-derived hydroxy epoxides, Environ. Sci. Technol., 44, 6718–23, doi:10.1021/es1019228, 2010.

Cometto, P. M., Dalmasso, P. R., Taccone, R. A, Lane, S. I., Oussar, F., Daële, V., Mellouki, A., and Le Bras, G.: Rate coefficients for the reaction of OH with a series of unsaturated alcohols between 263 and 371 K, J. Phys. Chem. A, 112, 4444–4450, doi:10.1021/jp7111186, 2008.

Curtiss, L. A., Raghavachari, K., Trucks, G. W., and Pople, J. A.: Gaussian-2 theory for molecular energies of first- and second-row compounds, J. Chem. Phys., 94, 7221–7230, 1991.

Darer, A. I., Cole-Filipiak, N. C., O'Connor, A. E., and Elrod, M. J.: Formation and stability of atmospherically relevant isoprene-derived organosulfates and organonitrates, Environ. Sci. Technol., 45, 1895–1902, doi:10.1021/es103797z, 2011.

Elrod, M. J.: Kinetics study of the aromatic bicyclic peroxy radical + NO reaction: overall rate constant and nitrate product yield measurements, J. Phys. Chem. A, 115, 8125–8130, doi:10.1021/jp204308f, 2011.

Fiore, A. M., Horowitz, L. W., Purves, D. W., Levy II, H., Evans, M. J., Wang, Y., Li, Q., and Yantosca, R. M.: Evaluating the contribution of changes in isoprene emissions to surface ozone trends over the eastern United States, J. Geophys. Res., 110, D12303, doi:10.1029/2004JD005485, 2005.

Frisch, M. J., Trucks, G. W., Schlegel, H. B., Scuseria, G. E., Robb, M. A., Cheeseman, J. R., Montgomery Jr., J. A., Vreven, T., Kudin, K. N., Burant, J. C., Millam, J. M., Iyengar, S. S., Tomasi, J., Barone, V., Mennucci, B., Cossi, M., Scalmani, G., Rega, N., Petersson, G. A., Nakatsuji, H., Hada, M., Ehara, M., Toyota, K., Fukuda, R., Hasegawa, J., Ishida, M., Nakajima, T., Honda, Y., Kitao, O., Nakai, H., Klene, M., Li, X., Knox, J. E., Hratchian, H. P., Cross, J. B., Bakken, V., Adamo, C., Jaramillo, J., Gomperts,

R., Stratmann, R. E., Yazyev, O., Austin, A. J., Cammi, R., Pomelli, C., Ochterski, J. W., Ayala, P. Y., Morokuma, K., Voth, G. A., Salvador, P., Dannenberg, J. J., Zakrzewski, V. G., Dapprich, S., Daniels, A. D., Strain, M. C., Farkas, O., Malick, D. K., Rabuck, A. D., Raghavachari, K., Foresman, J. B., Ortiz, J. V., Cui, Q., Baboul, A. G., Clifford, S., Cioslowski, J., Stefanov, B. B., Liu, G., Liashenko, A., Piskorz, P., Komaromi, I., Martin, R. L., Fox, D. J., Keith, T., Al-Laham, M. A., Peng, C. Y., Nanayakkara, A., Challacombe, M., Gill, P. M. W., Johnson, B., Chen, W., Wong, M. W., Gonzalez, C. and Pople, J. A.: Gaussian 03, 2004.

Froese, R. D. J., Svensson, M., and Morokuma, K.: IMOMO(G2MS): A New High-Level G2-Like Method for Large Molecules and Its Applications to Diels-Alder Reactions, J. Phys. Chem. A, 101, 227–233, 1997.

Guenther, A., Karl, T., Harley, P., Wiedinmyer, C., Palmer, P. I., and Geron, C.: Estimates of global terrestrial isoprene emissions using MEGAN (Model of Emissions of Gases and Aerosols from Nature), Atmos. Chem. Phys., 6, 3181–3210, doi:10.5194/acp-6-3181-2006, 2006.

Holloway, A.-L., Treacy, J., Sidebottom, H., Mellouki, A., Daële, V., Le Bras, G., and Barnes, I.: Rate coefficients for the reactions of OH radicals with the keto/enol tautomers of 2,4-pentanedione and 3-methyl-2,4-pentanedione, allyl alcohol and methyl vinyl ketone using the enols and methyl nitrite as photolytic sources of OH, J. Photochem. Photobio. A, 176, 183–190, doi:10.1016/j.jphotochem.2005.08.031, 2005.

Horowitz, L. W., Fiore, A. M., Milly, G. P., Cohen, R. C., Perring, A., Wooldridge, P. J., Hess, P. G., Emmons, L. K., and Lamarque, J.-F.: Observational constraints on the chemistry of isoprene nitrates over the eastern United States, J. Geophys. Res., 112, D12S08, doi:10.1029/2006JD007747, 2007.

Hu, K. S., Darer, A. I., and Elrod, M. J.: Thermodynamics and kinetics of the hydrolysis of atmospherically relevant organonitrates and organosulfates, Atmos. Chem. Phys., 11, 8307–8320, doi:10.5194/acp-11-8307-2011, 2011.

Jacobs, M. I., Darer, A. I., and Elrod, M. J.: Rate constants and products of the OH reaction with isoprene-derived epoxides, Environ. Sci. Technol., 47, 12868–12876, 2013.

Lee, L., Teng, A. P., Wennberg, P. O., Crounse, J. D., and Cohen, R. C.: On Rates and Mechanisms of OH and O_3 Reactions with Isoprene-Derived Hydroxy Nitrates., J. Phys. Chem. A, 118, 1622–1637, doi:10.1021/jp4107603, 2014.

Lin, Y.-H., Zhang, Z., Docherty, K. S., Zhang, H., Budisulistiorini, S. H., Rubitschun, C. L., Shaw, S. L., Knipping, E. M., Edgerton, E. S., Kleindienst, T. E., Gold, A., and Surratt, J. D.: Isoprene epoxydiols as precursors to secondary organic aerosol formation: acid-catalyzed reactive uptake studies with authentic compounds, Environ. Sci. Technol., 46, 250–258, doi:10.1021/es202554c, 2012.

Lockwood, A. L., Shepson, P. B., Fiddler, M. N., and Alaghmand, M.: Isoprene nitrates: preparation, separation, identification, yields, and atmospheric chemistry, Atmos. Chem. Phys., 10, 6169–6178, doi:10.5194/acp-10-6169-2010, 2010.

Lou, Y. R.: Comprehensive Handbook of Chemical Bond Energies, CRC Press, Boca Raton, FL, 2007.

Orlando, J. J., Tyndall, G. S., and Ceazan, N.: Rate Coefficients and Product Yields from Reaction of OH with 1-Penten-3-ol, (Z)-2-Penten-1-ol, and Allyl Alcohol (2-Propen-1-ol), J. Phys. Chem. A, 105, 3564–3569, doi:10.1021/jp0041712, 2001.

Patchen, A. K., Pennino, M. J., Kiep, A. C., and Elrod, M. J.: Direct Kinetics Study of the Product-Forming Channels of the Reaction of Hydroxyperoxy Radicals with NO, Int. J. Chem. Kinet., 39, 353–361, doi:10.1002/kin20248, 2007.

Paulot, F., Crounse, J. D., Kjaergaard, H. G., Kroll, J. H., Seinfeld, J. H., and Wennberg, P. O.: Isoprene photooxidation: new insights into the production of acids and organic nitrates, Atmos. Chem. Phys., 9, 1479–1501, doi:10.5194/acp-9-1479-2009, 2009a.

Paulot, F., Crounse, J. D., Kjaergaard, H. G., Kürten, A., St Clair, J. M., Seinfeld, J. H., and Wennberg, P. O.: Unexpected epoxide formation in the gas-phase photooxidation of isoprene, Science, 325, 730–733, doi:10.1126/science.1172910, 2009b.

Paulot, F., Henze, D. K., and Wennberg, P. O.: Impact of the isoprene photochemical cascade on tropical ozone, Atmos. Chem. Phys., 12, 1307–1325, doi:10.5194/acp-12-1307-2012, 2012.

Le Person, A., Solignac, G., Oussar, F., Daële, V., Mellouki, A., Winterhalter, R., and Moortgat, G. K.: Gas phase reaction of allyl alcohol (2-propen-1-ol) with OH radicals and ozone, Phys. Chem. Chem. Phys., 11, 7619–7628, doi:10.1039/b905776e, 2009.

Rindelaub, J. D., McAvey, K. M., and Shepson, P. B.: Determination of α-pinene-derived organic nitrate yields: particle phase partitioning and hydrolysis, Atmos. Chem. Phys. Discuss., 14, 3301–3335, doi:10.5194/acpd-14-3301-2014, 2014.

Rollins, A. W., Pusede, S., Wooldridge, P., Min, K. E., Gentner, D. R., Goldstein, a. H., Liu, S., Day, D. A., Russell, L. M., Rubitschun, C. L., Surratt, J. D., and Cohen, R. C.: Gas/particle partitioning of total alkyl nitrates observed with TD-LIF in Bakersfield, J. Geophys. Res. Atmos., 118, 6651–6662, doi:10.1002/jgrd.50522, 2013.

Seeley, J. V., Jayne, J. T., and Molina, M. J.: High pressure fast-flow technique for gas phase kinetics studies, Int. J. Chem. Kinet., 25, 571–594, 1993.

Sprengnether, M., Demerjian, K. L., Donahue, N. M., and Anderson, J. G.: Product analysis of the OH oxidation of isoprene and 1, 3-butadiene in the presence of NO, J. Geophys. Res., 107, 4268, doi:10.1029/2001JD000716, 2002.

Surratt, J. D., Chan, A. W. H., Eddingsaas, N. C., Chan, M., Loza, C. L., Kwan, A. J., Hersey, S. P., Flagan, R. C., Wennberg, P. O., and Seinfeld, J. H.: Reactive intermediates revealed in secondary organic aerosol formation from isoprene, P. Natl. Acad. Sci. USA, 107, 6640–6645, doi:10.1073/pnas.0911114107, 2010.

Treves, K. and Rudich, Y.: The Atmospheric Fate of C3–C6 Hydroxyalkyl Nitrates, J. Phys. Chem. A, 107, 7809–7817, 2003.

von Kuhlmann, R., Lawrence, M. G., Pöschl, U., and Crutzen, P. J.: Sensitivities in global scale modeling of isoprene, Atmos. Chem. Phys., 4, 1–17, doi:10.5194/acp-4-1-2004, 2004.

Wennberg, P. O.: Let's abandon the "high NOX" and "low NOX" terminology, IGAC News, 50 (July 2013), 3–4, 2013.

Whalen, D. L.: Mechanisms of Hydrolysis and Rearrangement of Epoxides, in: Advances in Physical Organic Chemistry, Vol. 40, edited by: Richards, J. P., 247–297, Academic Press, London, 2005.

Zhao, J. and Zhang, R.: Proton transfer reaction rate constants between hydronium ion (H_3O+) and volatile organic compounds, Atmos. Environ., 38, 2177–2185, doi:10.1016/j.atmosenv.2004.01.019, 2004.